Investigation of Martian magnetic topology response to 2017 September ICME

Shaosui Xu[1], Xiaohua Fang[2], David L. Mitchell[1], Yingjuan Ma[3], Janet G. Luhmann[1], Gina A. DiBraccio[4], Tristan Weber[2], David Brain[2], Christian Mazelle[5], Shannon M. Curry[1], and Christina O. Lee[1]

Shaosui Xu, shaosui.xu@berkeley.edu

[1]Space Sciences Laboratory, University of California, Berkeley, USA

[2]Laboratory for Atmospheric and Space Physics, University of Colorado, Boulder, Colorado, USA

[3]Institute of Geophysics and Planetary Physics, University of California, Los Angeles, California, USA

[4]Goddard Space Flight Center, Greenbelt, Maryland, USA

This article has been accepted for publication and undergone full peer review but has not been through the copyediting, typesetting, pagination and proofreading process, which may lead to differences between this version and the Version of Record. Please cite this article as doi: 10.1002/2018GL077708

Many aspects of the Sun-Mars interaction have been investigated during solar transient events with measurements from multiple spacecrafts and also simulation efforts. Limited discussion has been paid to magnetic topology response to disturbed upstream conditions. The implications of topology changes include, but are not limited to, the pattern of energetic particle precipitation into the Martian atmosphere and the impact on cold ion escape during solar transient events as low energy ion escape is dependent on magnetic topology. In this study, we investigate the magnetic topology response to the 2017 September interplanetary coronal mass ejection (ICME) event with measurements collected by the Mars Atmospheric and Volatile EvolutioN (MAVEN) spacecraft. It is found that the interface between draped IMF and closed field lines was moved from $800-1400$ km in altitude during quiet conditions to 200-400 km after ICME arrived at Mars, then relaxed back to high altitudes again after the event. To gain insight into magnetic topology response on a global scale, we first validate magnetic topology from a time-dependent simulation with a single-fluid multi-species magnetohydrodynamic (MHD) model by comparing magnetic topology determined from MAVEN data, which shows a good agreement. Then we present MHD predictions of global magnetic topol-

[5]IRAP, CNRS - University of Toulouse - UPS - CNES, Toulouse, France

ogy changes during this ICME event. In addition to a deeper IMF penetration, MHD results suggest more open field lines in response to the ICME event.

Keypoints:

- From MAVEN data, IMF is found to penetrate deeper over the northern hemisphere due to enhanced solar wind dynamic pressure during the ICME
- Topology from MHD shows a good agreement with data and provides insights into a global response
- MHD results suggest deeper IMF penetration and more open field lines during the ICME event

1. Introduction

Mars possesses localized crustal magnetic fields [*Acuña et al.*, 1998; *Acuna et al.*, 1999; *Connerney et al.*, 2005, 2015a] that, together with the ionosphere, present a complex obstacle to the solar wind. The investigation of Mars' response to major space weather events is an important aspect of understanding general planetary solar wind interactions as well as constraining Martian atmosphere loss to space over time. Previous studies have been dedicated to the effects of solar wind stream interaction regions (SIRs) and interplanetary coronal mass ejections (ICMEs) using data from Phobos-2 [e.g. *McKenna-Lawlor et al.*, 2005], Mars Global Surveyor (MGS) [e.g. *Crider et al.*, 2005; *Vennerstrom*, 2011], Mars Express (MEX) [e.g. *Dubinin et al.*, 2009; *Edberg et al.*, 2009, 2010; *Opgenoorth et al.*, 2013; *Morgan et al.*, 2014; *Ramstad et al.*, 2017], and MAVEN [e.g. *Jakosky et al.*, 2015a]. The reported influences include, but are not limited to, enhanced magnetic field pileup around Mars, plasma boundaries being pushed to lower altitude, and increases in ion escape rate. Meanwhile, simulation efforts have also been made in studying global effects of solar transient events on the Martian plasma environment [e.g. *Fang et al.*, 2013; *Jakosky et al.*, 2015a; *Dong et al.*, 2015; *Curry et al.*, 2015; *Luhmann et al.*, 2017; *Ma et al.*, 2017] [Romanelli et al., this issue, MS#2018GL077714].

Limited discussion in literature has been paid to magnetic topology, which is a key aspect of the Mars response. The mapping of Martian magnetic topology under quiet solar wind conditions has been performed with MGS [e.g. *Mitchell et al.*, 2001; *Brain et al.*, 2005, 2007; *Xu et al.*, 2014; *Shane et al.*, 2016], MEX [e.g. *Frahm et al.*, 2006; *Liemohn et al.*, 2006a, b, 2007; *Frahm et al.*, 2010], and MAVEN [e.g. *Steckiewicz et al.*, 2015, 2017;

Xu et al., 2016a, 2017a, b; *Garnier et al.*, 2017; *Weber et al.*, 2017]. For disturbed solar wind conditions, *Crider et al.* [2005] showed that solar wind/magnethosheath electrons overwhelmed MGS observational altitudes ($\sim$ 400 km) during the Halloween ICME event, in lieu of ionospheric photoelectrons typically observed under quiet conditions. This observation suggests that the photoelectron boundary (PEB, [e.g. *Mitchell et al.*, 2001; *Garnier et al.*, 2017]) was pushed below MGS altitudes in response to ICME. However, *Crider et al.* [2005] only examined omni-directional electron fluxes so that there exists an ambiguity of whether this IMF (interplanetary magnetic field) penetration is simply draping or due to an increase of "open" Martian magnetic field topology.

Here, we define an open field line as one end being embedded in the ionosphere below 160-200 km (or the superthermal electron exobase, [e.g. *Xu et al.*, 2016b, 2017a]) with the other end connecting to the solar wind. This definition differentiates whether a field line is connected to the ionosphere below the exobase, which is important to characterize ion escape. Cold ion (with a few eV energy) escape likely operates on different mechanisms for different magnetic topologies [e.g. *Lillis et al.*, 2015]. Closed field lines trap low-energy ions; open field lines allow polar-wind like ionospheric outflow, mainly driven by ambipolar electric fields [e.g. *Collinson et al.*, 2015]; draped field lines scrape away ions, mainly accelerated by the $\mathbf{J} \times \mathbf{B}$ force and convection electric field [e.g. *Fang et al.*, 2008; *Halekas et al.*, 2017]. In addition, *Luhmann et al.* [2017] examined Mars' response to ICMEs with simulations from a single-fluid multi-species magnetohydrodynamic (MHD) model [*Ma et al.*, 2002, 2004] and found that during ICMEs, there are more open field lines from simulation results, possibly responsible for a factor of a few to 1-2 orders of

magnitude enhancement in ion escape rate. Therefore, the investigation of magnetic topology response is important to characterize the impact of space weather events on cold ion escape.

With comprehensive plasma and field data collected by the MAVEN spacecraft [*Jakosky et al.*, 2015b], we characterize magnetic topology response to the 2017 September ICME event in a more accurate way by examining measurements from Solar Wind Electron Analyzer (SWEA, [*Mitchell et al.*, 2016]) and Magnetometer data (MAG, [*Connerney et al.*, 2015b]). However, MAVEN only provides measurements along its orbit. MHD modeling, though having its limitations in simulating some aspects of the Sun-Mars interaction, provides insight to magnetic topology on a global scale. In this study, we first compare magnetic topology determined from MAVEN data with that from a time-dependent simulation with the single-fluid multi-species MHD model [Ma et al., MS# 2018GL077707, this issue] to validate MHD results. Then we use the MHD model results to picture the global magnetic topology response to this ICME event.

2. Methodology and Orbit Example

Superthermal electrons have been used as magnetic tracers to deduce magnetic topology at Mars based on two basic principles: (1) a loss-cone pitch angle distribution (a significant depletion/absorption of electrons in more field-aligned directions compared to more perpendicular directions) implies the field line intersecting the collisional atmosphere [e.g. *Brain et al.*, 2007; *Weber et al.*, 2017]; (2) the presence of ionospheric photoelectrons indicates the footpoint(s) of a field line embedded in the dayside ionosphere [e.g. *Xu et al.*, 2017a]. For one single electron and magnetic field measurement, we can separate

superthermal electrons with velocities pointing "toward" or "away from" Mars. Sequentially, for each direction, if a loss cone and/or photoelectrons is (are) detected, we can determine if the field line connects to the atmosphere once, twice, or not at all, corresponding to open, closed, and draped fields respectively. In addition, on the nightside, superthermal electron voids have been observed [e.g. *Mitchell et al.*, 2001; *Steckiewicz et al.*, 2017], resulting from a lack of solar photoionization sourcing within the optical shadow and continuous loss to the atmosphere mainly via electron-neutral inelastic collision. A more detailed methodology using pitch angle distributions (PADs) to determine magnetic topology can be found in section 2 of *Brain et al.* [2007]. The usage of photoelectrons inferring topology is described in detail in section 3 of *Xu et al.* [2017a]. In this study, we determine the magnetic topology with a combination of the two techniques.

Figure 1 shows MAVEN measurements and derived quantities on Sep. 12, 2017. Figure 1e presents the pitch-angle resolved shape parameters [*Xu et al.*, 2017a]. A canonical photoelectron spectrum has sharp features [e.g. *Liemohn et al.*, 2003; *Xu et al.*, 2015a; *Peterson et al.*, 2016], such as: (1) a cluster of peaks from 22-27 eV from 30.4 nm He II solar line ionizing CO_2 and O; (2) a sharp flux drop from 60 to 70 eV (termed "the photoelectron knee"), corresponding to a sharp decrease of solar irradiance at wavelengths shorter than 17 nm. As described in section 4 of *Xu et al.* [2017a], a shape parameter is the difference of the derivative electron flux of a measured electron spectrum and of a canonical ionospheric photoelectron spectrum. The smaller a shape parameter is, the more likely it is to be photoelectrons. Following *Xu et al.* [2017a], we define shape parameter < 1 as photoelectrons and shape parameter > 1 as solar wind electrons (or

non-photoelectrons). "Toward" and "away" refer to electrons with velocities pointing toward or away from Mars in this study. In particular, for positive magnetic elevation angles (relative to the horizontal plane), "toward" and "away" indicate pitch angles $135° - 180°$ and $0 - 45°$, respectively; for negative elevation angles, "toward" and "away" indicate pitch angles $0 - 45°$ and $135° - 180°$, respectively.

Sequentially, closed field lines can be defined as photoelectrons observed traveling in both directions or shape parameters for both "toward" and "away" directions below 1, e.g. near periapsis below 200 km (UT 22:50-23:00), shown as red in Figure 1g correspondingly. Open is defined as photoelectrons traveling away from Mars and solar wind electrons traveling toward Mars, or "away" shape parameter < 1 and "toward" shape parameter > 1, e.g. UT 22:45 - 22:50, colored as green in Figure 1g.

One caveat of this two-stream shape parameter method is that, for cases with shape parameters > 1 in both directions, it can be either draped field lines or open field lines. For an open field connecting to the nightside atmosphere, both incoming solar wind electrons and backscattered electrons will result in a shape parameter > 1, which is the same in terms of shape parameter alone for draped field lines. Another complication occurs during disturbed solar wind conditions when the incoming solar wind electron flux is so high that the backscattered electron flux skews/masks photoelectron spectral features. Both scenarios can be compensated by taking into account the electron flux ratio of "away" and "toward" directions, as shown in Figure 1f. When a field line intersects the collisional atmosphere, the incident electrons (in the "toward" direction) are mostly absorbed by the atmosphere and therefore the outward electrons (in the "away" direction) consist of

backscattered electrons within loss-cone pitch angles. As shown in *Collinson et al.* [2016], the backscattered electron flux is typically $10\% - 30\%$ of incident electron flux estimated from both SWEA measurements and simulation results with the Superthermal Electron Transport (STET) model [*Xu and Liemohn*, 2015; *Xu et al.*, 2015b]. In other words, when a loss cone is present, the electron flux ratio of "away" and "toward" directions is around $10\%-30\%$. Because the loss cone width is variable and not known a priori and also dayside photoelectron fluxes (in the "away" direction) might raise the ratio, we set an electron-flux-ratio threshold of 0.8 for 100-300 eV electrons for whether a loss cone is detected. In other words, for cases with shape parameters > 1 in both directions, if the away-to-toward flux ratio is less than (greater than) 0.8, it is defined as open (draped). For example, at UT 23:12 - 23:16, the "toward" electrons are undoubtedly solar wind electrons with shape parameters > 1, the "away" shape parameter is slightly above 1 because photoelectron spectra are skewed by high backscattered solar wind electron flux. Meanwhile, loss cones are present in Figure 1c and also the flux ratio is around 0.5 in Figure 1f. This period is identified as open because of this additional criterion, correspondingly colored in green in Figure 1g.

3. Magnetic Topology Response to ICME

With shape parameters to pick out photoelectrons and flux ratios to identify loss cones, magnetic topology can be determined throughout the event. Figure 2 shows the orbit geometry and magnetic topology from Sep. 7 to Sep. 17, 2017, corresponding to orbit numbers 5698-5751. For this event, the ICME shock arrival occurred at 2017-09-13/02:52 (orbit 5731) and solar wind dynamic pressure enhancement due to ICME lasted for approx-

imately two days, roughly ending on orbit 5742 [Lee et al., this issue, MS#2018GL077917]. In addition, a SIR encounter happened around orbit 5720 (periapsis at 2017-09-11/02:34) and is discussed in more details in Lee et al. [this issue, MS#2018GL077917]. During these ten days, MAVEN was mostly collecting data near the terminator plane (Figures 2b-2d) and the periapsis is over the northern high latitudes (Figure 2a). This orbit geometry is convenient to study magnetic topology: inbound segments over the weak crustal field regions and outbound segments over the north pole. In other words, the magnetic topology is less affected by local crustal fields, unlike the highly longitudinal-dependent southern strong crustal field regions. It is worth noting that localized crustal magnetic anomalies have been found to possess a global influence even in the northern hemisphere [e.g. *Brain et al.*, 2006; *Xu et al.*, 2017a; *Fang et al.*, 2017, 2018]

A convenient way to exhibit topology changes throughout the event is displayed in Figure 2e, where magnetic topologies along the low-altitude part of the orbits are stacked up. Solar wind conditions were considered to be quiet prior to the SIR encounter where the draped IMF extends down to ∼600 km inbound and ∼1000 km outbound. The solar wind dynamic pressure was low at this time (<1 nPa), effectively even lower near the terminator, so that over the northern hemisphere, the interface between draped IMF and closed field lines is located at relatively high altitudes to account for the pressure balance. Four days (Sep. 07 to Sep. 10, orbits 5698-5719) of magnetic topology under quiet conditions, spanning over longitudes $0 - 360°$, are displayed to set a baseline regardless of crustal field patches over the north.

When solar wind is disturbed, draped fields are pushed to lower altitudes, in particular for orbits 5720 and orbits 5731-5742. On orbit 5720 (during the SIR encounter), IMF penetration was lowered to ∼300 km outbound while this altitude is uncertain for inbound due to insufficient pitch angle coverage near periapsis. Immediately after the shock arrival (orbit 5731), the periapsis passage experienced the deepest IMF penetration, with closed field lines extending only up to 200 km in both the inbound and outbound directions. In addition, the spacecraft was passing near the terminator where field lines are more likely to be horizontal to the surface. In such a case, the superthermal electron exobase can reach altitudes up to 200 km, comparing to a nominal exobase altitude of ∼160 km for vertical magnetic fields, as shown in Figure 12a of *Xu et al.* [2017a]. In other words, for magnetic elevation angle less than $5^\circ - 10^\circ$, the field lines can be open or deeply draped below 200 km even though our technique, based on electron data and only valid above the exobase, determines it to be closed. Therefore, readers should be aware of the large uncertainty to the magnetic topology in this study below 200 km near the terminator.

Despite caveats, Figure 2e clearly manifests the magnetic topology response to disturbed solar wind: IMF that drapes at high altitudes ($> 600 - 1000$ km) during quiet time (orbits 5698-5719), penetrates to low altitudes (as low as ~ 200 km) during SIR (orbits 5720) and ICMEs passages (orbits 5731-5742) due to increased upstream dynamic pressure and/or larger IMF strength, and relaxes to higher altitudes afterwards (orbits 5720-5730 and 5742-5751).

4. Data-Model Comparison of Magnetic Topology

Due to measurement constraints based on MAVEN's single-point observations and limited time in the northern hemisphere during a given orbit, it is challenging to globally contextualize the magnetic topology response to solar events. To gain some insight into magnetic topology response to the ICME event on a global scale, we examine results from a time-dependent simulation for this event with the single-fluid multi-species MHD model. As MAVEN was mostly sampling within the bow shock and does not provide direct upstream measurements, the solar wind input for this simulation is derived from sheath measurements and filled with linear interpolation between inbound and outbound sheath estimates for inside the magnetic pileup boundary. Details of the model and simulation setup can be found in Ma et al. [this issue, MS# 2018GL077707]. We first compare magnetic topology determined from the MAVEN data with that from MHD to validate MHD results and then present MHD predictions of global and temporal magnetic topology response. The field lines are traced within the MHD simulation results on a 5-minute cadence along the MAVEN trajectory.

Figure 3 shows the comparison of magnetic topology from MAVEN and MHD for low-altitude segments of orbits right before the shock (5730), immediately after the ICME shock (5731), and one orbit after (5732). For orbit 5730 (Figure 3a), magnetic topology from MHD agrees well with that from MAVEN below 600 km inbound and 800 km outbound, despite the more structured data. The discrepancy from UT 22:30-22:40 is mainly because there is a rotation in measured magnetic fields (see Figure 1b), probably due to an IMF rotation, that is not captured in the MHD input. For the orbit after the shock (5731,

Figure 3b), magnetic topology from both data and model show that IMF penetrates down to 400 km inbound and 600-700 km outbound, and closed field lines extend only up to 200-300 km with open field lines in between. Some draped IMF penetrates even down to 200 km according to MAVEN data. For orbit 5732 (Figure 3c), both MAVEN and MHD results show that IMF penetrates down to 300-400 km due to continuing enhanced dynamic pressure from the ICME. The main discrepancy is that MHD mostly predicts open field lines for this periapsis passage while MAVEN data suggests mostly closed. Notice that below 200 km, topology determined from electron data has an uncertainty due to a raised electron exobase. Overall, considering that the MHD inputs are mostly derived quantities and might miss some fast changes in real upstream drivers, magnetic topology from MHD is in a reasonable good agreement with data.

Now that we have established that MHD provides good magnetic topology predictions by comparing with MAVEN data, especially for the orbits before and after the shock arrival, we can compare the magnetic topology from MHD for these two orbits to examine the global response to the ICME event, as shown in Figure 4. Before the shock arrival (Figure 4a), the northern hemisphere is covered by closed, open, and some draped fields at 350 km. In the southern hemisphere (Figure 4b), closed field lines dominate at 350 km because of strong crustal fields. In contrast, after the shock arrival, more IMF penetration to 350 km and more open fields are seen over the north (Figure 4c) and the southern hemisphere is populated with more open field lines (Figure 4d). Though partly attributed to different crustal field orientations before/after the shock, more open field lines during an ICME encounter is consistent with the findings of *Luhmann et al.* [2017], caused by

a combination of magnetic reconnection between IMF and crustal fields [e.g. Harada et al., accepted, MS#2018GL077281] and also open field lines being pushed to low altitudes due to high dynamic pressure. Note that the main topology change in response to the ICME from MHD results is more open field lines, in contrast to more IMF penetration from MAVEN data. It is probably because MAVEN's periapsis segments were limited to the dusk terminator over the northern high latitudes so that MAVEN topology results might not be representative for a global picture.

5. Discussion and Conclusions

In this study, we determine magnetic topology before/during/after the 2017 Sept ICME encounter with MAVEN superthermal electron and magnetic field data. The magnetic topology response to the ICME event is clearly shown: the interface between draped IMF and closed field lines is seen to move roughly from 834±203 (standard deviation) km to 300 km inbound and from 1390±490 km to 200-400 km outbound after the ICME arrived at Mars, then relaxed back to high altitudes after the event.

Magnetic topology is closely related to cold ion escape; different mechanisms operate on different topologies for these low energy ions. Closed field lines trap cold ions; open field lines intersect the ionosphere below the exobase, where ion densities are high and allow ion escape along the field lines; draped field lines carry away ions at altitudes above the ion exobase. During the ICME and also the SIR encounter, IMF penetrates deeper into the Martian atmosphere due to enhanced dynamic pressure while closed field lines are compressed to lower altitudes, which could indicate that ions are subject to escape

through open field lines and draped IMF starting from lower altitudes, where ion densities are higher.

However, the MAVEN observations analyzed here have periapsis limited to northern latitudes and the dusk terminator due to its orbit geometry. The magnetic topology response on a global scale is determined by examining a time-dependent MHD simulation for this event. We first compare the topology from MHD with MAVEN observations, which shows a good agreement and validates the topology results from MHD. As suggested by the limited MAVEN perspective, the comparison of global magnetic topology from MHD at 350 km before and after the shock arrival shows more IMF penetration over the northern high latitudes, consistent with MAVEN data. Additionally, at 350 km, more open field lines are seen all over the planet due to a combination of different crustal field orientations and possibly higher reconnection rate between IMF and crustal fields. This exercise not only demonstrates that the MHD model is an excellent tool to simulate magnetic topology at Mars, even during disturbed conditions, but also provides a more comprehensive picture of how the topology responds on a global scale to this ICME event.

Acknowledgments. The work was supported by the NASA MAVEN project through the Mars Exploration Program. The MAVEN data used in this study are available through Planetary Data System (http://ppi.pds. nasa.gov/mission/MAVEN). The BATS-R-US code is publicly available from http://csem.engin.umich.edu/ tools/swmf. For the distribution of the model results used in this study, please contact Dr. X. Fang (Xiaohua.Fang@colorado.edu).

References

Acuña, M., J. Connerney, P. a. Wasilewski, R. Lin, K. Anderson, C. Carlson, J. McFadden, D. Curtis, D. Mitchell, H. Reme, et al. (1998), Magnetic field and plasma observations at Mars: Initial results of the Mars Global Surveyor mission, *Science*, *279*(5357), 1676–1680.

Acuna, M., J. Connerney, R. Lin, D. Mitchell, C. Carlson, J. McFadden, K. Anderson, H. Rème, C. Mazelle, D. Vignes, et al. (1999), Global distribution of crustal magnetization discovered by the Mars Global Surveyor MAG/ER experiment, *Science*, *284*(5415), 790–793.

Brain, D., J. Halekas, R. Lillis, D. Mitchell, R. Lin, and D. Crider (2005), Variability of the altitude of the Martian sheath, *Geophysical Research Letters*, *32*(18).

Brain, D., R. Lillis, D. Mitchell, J. Halekas, and R. Lin (2007), Electron pitch angle distributions as indicators of magnetic field topology near Mars, *Journal of Geophysical Research: Space Physics (1978–2012)*, *112*(A9).

Brain, D. A., D. L. Mitchell, and J. S. Halekas (2006), The magnetic field draping direction at Mars from April 1999 through August 2004, *Icarus*, *182*(2), 464–473.

Collinson, G., D. Mitchell, A. Glocer, J. Grebowsky, W. K. Peterson, J. Connerney, L. Andersson, J. Espley, C. Mazelle, J.-A. Sauvaud, A. Fedorov, Y. Ma, S. Bougher, R. Lillis, R. Ergun, and B. Jakosky (2015), Electric Mars: The first direct measurement of an upper limit for the Martian "polar wind" electric potential, *Geophysical Research Letters*, *42*(21), 9128–9134, doi:10.1002/2015GL065084, 2015GL065084.

Collinson, G., D. Mitchell, S. Xu, A. Glocer, J. Grebowsky, T. Hara, R. Lillis, J. Espley, C. Mazelle, J.-A. Sauvaud, et al. (2016), Electric Mars: A large trans-terminator electric potential drop on closed magnetic field lines above Utopia Planitia, *Journal of Geophysical Research: Space Physics*.

Connerney, J., M. Acuña, N. Ness, G. Kletetschka, D. Mitchell, R. Lin, and H. Reme (2005), Tectonic implications of Mars crustal magnetism, *Proceedings of the national Academy of Sciences of the United States of America*, *102*(42), 14,970–14,975.

Connerney, J., J. Espley, R. Oliversen, D. Sheppard, and G. Dibraccio (2015a), First Results from the MAVEN Magnetic Field Investigation, in *Lunar and Planetary Science Conference*, vol. 46, p. 1080.

Connerney, J., J. Espley, P. Lawton, S. Murphy, J. Odom, R. Oliversen, and D. Sheppard (2015b), The MAVEN magnetic field investigation, *Space Science Reviews*, pp. 1–35.

Crider, D. H., J. Espley, D. A. Brain, D. L. Mitchell, J. E. P. Connerney, and M. H. Acua (2005), Mars Global Surveyor observations of the Halloween 2003 solar superstorm's encounter with Mars, *Journal of Geophysical Research: Space Physics*, *110*(A9), n/a–n/a, doi:10.1029/2004JA010881, a09S21.

Curry, S. M., J. G. Luhmann, Y. J. Ma, C. Dong, D. Brain, F. Leblanc, R. Modolo, Y. Dong, J. McFadden, J. Halekas, et al. (2015), Response of Mars O+ pickup ions to the 8 March 2015 ICME: Inferences from MAVEN data-based models, *Geophysical Research Letters*, *42*(21), 9095–9102.

Dong, C., Y. Ma, S. W. Bougher, G. Toth, A. F. Nagy, J. S. Halekas, Y. Dong, S. M. Curry, J. G. Luhmann, D. Brain, et al. (2015), Multifluid MHD study of the solar wind interaction with Mars' upper atmosphere during the 2015 March 8th ICME event, *Geophysical Research Letters*, *42*(21), 9103–9112.

Dubinin, E., M. Fraenz, J. Woch, F. Duru, D. Gurnett, R. Modolo, S. Barabash, and R. Lundin (2009), Ionospheric storms on Mars: Impact of the corotating interaction region, *Geophysical Research Letters*, *36*(1), n/a–n/a, doi:10.1029/2008GL036559, l01105.

Edberg, N. J., U. Auster, S. Barabash, A. Bößwetter, D. A. Brain, J. L. Burch, C. M. Carr, S. W. H. Cowley, E. Cupido, F. Duru, A. I. Eriksson, M. Fränz, K.-H. Glassmeier, R. Goldstein, M. Lester, R. Lundin, R. Modolo, H. Nilsson, I. Richter, M. Samara, and J.-G. Trotignon (2009), Rosetta and Mars Express observations of the influence of high solar wind pressure on the Martian plasma environment, *Annales Geophysicae*, *27*(12), 4533–4545.

Edberg, N. J. T., H. Nilsson, A. O. Williams, M. Lester, S. E. Milan, S. W. H. Cowley, M. Fr?nz, S. Barabash, and Y. Futaana (2010), Pumping out the atmosphere of Mars through solar wind pressure pulses, *Geophysical Research Letters*, *37*(3), n/a–n/a, doi: 10.1029/2009GL041814, l03107.

Fang, X., M. W. Liemohn, A. F. Nagy, Y. Ma, D. L. De Zeeuw, J. U. Kozyra, and T. H. Zurbuchen (2008), Pickup oxygen ion velocity space and spatial distribution around Mars, *Journal of Geophysical Research: Space Physics*, *113*(A2).

Fang, X., S. W. Bougher, R. E. Johnson, J. G. Luhmann, Y. Ma, Y.-C. Wang, and M. W. Liemohn (2013), The importance of pickup oxygen ion precipitation to the Mars upper atmosphere under extreme solar wind conditions, *Geophysical Research Letters*, *40*(10), 1922–1927.

Fang, X., Y. Ma, K. Masunaga, Y. Dong, D. Brain, J. Halekas, R. Lillis, B. Jakosky, J. Connerney, J. Grebowsky, et al. (2017), The Mars crustal magnetic field control of plasma boundary locations and atmospheric loss: MHD prediction and comparison with MAVEN, *Journal of Geophysical Research: Space Physics*, *122*(4), 4117–4137.

Fang, X., Y. Ma, J. G. Luhmann, Y. Dong, D. A. Brain, D. M. Hurley, C. Dong, C. O. Lee, and B. M. Jakosky (2018), The morphology of the solar wind magnetic field draping on the dayside of Mars and its variability, *Geophysical Research Letters*, *45*, doi: 10.1002/2018GL077230.

Frahm, R., J. Sharber, J. Winningham, P. Wurz, M. Liemohn, E. Kallio, M. Yamauchi, R. Lundin, S. Barabash, A. Coates, et al. (2006), Locations of atmospheric photoelectron energy peaks within the Mars environment, *Space Science Reviews*, *126*(1-4), 389–402.

Frahm, R., J. Sharber, J. Winningham, R. Link, M. Liemohn, J. Kozyra, A. Coates, D. Linder, S. Barabash, R. Lundin, et al. (2010), Estimation of the escape of photoelectrons from Mars in 2004 liberated by the ionization of carbon dioxide and atomic oxygen, *Icarus*, *206*(1), 50–63.

Garnier, P., M. Steckiewicz, C. Mazelle, S. Xu, D. Mitchell, M. K. G. Holmberg, J. S. Halekas, L. Andersson, D. A. Brain, J. E. P. Connerney, J. R. Espley, R. J. Lillis, J. G. Luhmann, J.-A. Sauvaud, and B. M. Jakosky (2017), The Martian Photoelectron Boundary as Seen by MAVEN, *Journal of Geophysical Research: Space Physics*, *122*(10), 10,472–10,485, doi:10.1002/2017JA024497, 2017JA024497.

Halekas, J., D. Brain, J. Luhmann, G. DiBraccio, S. Ruhunusiri, Y. Harada, C. Fowler, D. Mitchell, J. Connerney, J. Espley, et al. (2017), Flows, Fields, and Forces in the Mars-Solar Wind Interaction, *Journal of Geophysical Research: Space Physics*, *122*(11).

Jakosky, B. M., J. M. Grebowsky, J. G. Luhmann, J. Connerney, F. Eparvier, R. Ergun, J. Halekas, D. Larson, P. Mahaffy, J. Mcfadden, et al. (2015a), MAVEN observations of the response of Mars to an interplanetary coronal mass ejection, *Science*, *350*(6261), aad0210.

Jakosky, B. M., R. Lin, J. Grebowsky, J. Luhmann, D. Mitchell, G. Beutelschies, T. Priser, M. Acuna, L. Andersson, D. Baird, et al. (2015b), The Mars atmosphere and volatile evolution (MAVEN) mission, *Space Science Reviews*, *195*(1-4), 3–48.

Liemohn, M. W., D. L. Mitchell, A. F. Nagy, J. L. Fox, T. W. Reimer, and Y. Ma (2003), Comparisons of electron fluxes measured in the crustal fields at Mars by the MGS magnetometer/electron reflectometer instrument with a B field–dependent transport code, *Journal of Geophysical Research*, *108*(E12), 5134.

Liemohn, M. W., R. A. Frahm, J. D. Winningham, Y. Ma, S. Barabash, R. Lundin, J. U. Kozyra, A. F. Nagy, S. M. Bougher, J. Bell, D. Brain, D. Mitchell, J. Luhmann, M. Holmström, H. Andersson, M. Yamauchi, A. Grigoriev, S. McKenna-Lawler,

J. R. Sharber, J. R. Scherrer, S. J. Jeffers, A. J. Coates, D. R. Linder, D. O. Kataria, E. Kallio, H. Koskinen, T. Säles, P. Riihelä, W. Schmidt, E. Roelof, D. Williams, S. Livi, C. C. Curtis, K. C. Hsieh, B. R. Sandel, M. Grande, M. Carter, J.-A. Sauvaud, A. Fedorov, J.-J. Thocaven, S. Orsini, R. Cerulli-Irelli, M. Maggi, P. Wurz, P. Bochsler, N. Krupp, J. Woch, M. Fränz, K. Asamura, and C. Dierker (2006a), Numerical interpretation of high-altitude photoelectron observations, *ICARUS*, *182*, 383–395, doi: 10.1016/j.icarus.2005.10.036.

Liemohn, M. W., Y. Ma, R. A. Frahm, X. Fang, J. U. Kozyra, A. F. Nagy, J. D. Winningham, J. R. Sharber, S. Barabash, and R. Lundin (2006b), Mars Global MHD Predictions of Magnetic Connectivity Between the Dayside Ionosphere and the Magnetospheric Flanks, *Space Science Reviews*, *126*, 63–76, doi:10.1007/s11214-006-9116-8.

Liemohn, M. W., Y. Ma, A. Nagy, J. Kozyra, J. Winningham, R. Frahm, J. Sharber, S. Barabash, and R. Lundin (2007), Numerical modeling of the magnetic topology near Mars auroral observations, *Geophysical Research Letters*, *34*(24).

Lillis, R. J., D. A. Brain, S. W. Bougher, F. Leblanc, J. G. Luhmann, B. M. Jakosky, R. Modolo, J. Fox, J. Deighan, X. Fang, et al. (2015), Characterizing atmospheric escape from Mars today and through time, with MAVEN, *Space Science Reviews*, *195*(1-4), 357.

Luhmann, J., C. Dong, Y. Ma, S. Curry, S. Xu, C. Lee, T. Hara, J. Halekas, Y. Li, J. Gruesbeck, et al. (2017), Martian Magnetic Storms, *Journal of Geophysical Research: Space Physics*.

Ma, Y., A. F. Nagy, K. C. Hansen, D. L. DeZeeuw, T. I. Gombosi, and K. Powell (2002), Three-dimensional multispecies MHD studies of the solar wind interaction with Mars in the presence of crustal fields, *Journal of Geophysical Research: Space Physics (1978–2012)*, *107*(A10), 1282–1289.

Ma, Y., A. F. Nagy, I. V. Sokolov, and K. C. Hansen (2004), Three-dimensional, multispecies, high spatial resolution MHD studies of the solar wind interaction with Mars, *Journal of Geophysical Research: Space Physics (1978–2012)*, *109*(A7).

Ma, Y. J., C. T. Russell, X. Fang, C. F. Dong, A. F. Nagy, G. Toth, J. S. Halekas, J. E. P. Connerney, J. R. Espley, P. R. Mahaffy, M. Benna, J. McFadden, D. L. Mitchell, L. Andersson, and B. M. Jakosky (2017), Variations of the Martian plasma environment during the ICME passage on 8 March 2015: A time-dependent MHD study, *Journal of Geophysical Research: Space Physics*, *122*(2), 1714–1730, doi:10.1002/2016JA023402, 2016JA023402.

McKenna-Lawlor, S. M. P., M. Dryer, C. D. Fry, W. Sun, D. Lario, C. S. Deehr, B. Sanahuja, V. A. Afonin, M. I. Verigin, and G. A. Kotova (2005), Predictions of energetic particle radiation in the close Martian environment, *Journal of Geophysical Research: Space Physics*, *110*(A3), n/a–n/a, doi:10.1029/2004JA010587, a03102.

Mitchell, D., R. Lin, C. Mazelle, H. Reme, P. Cloutier, J. Connerney, M. Acuña, and N. Ness (2001), Probing Mars' crustal magnetic field and ionosphere with the MGS Electron Reflectometer, *Journal of Geophysical Research: Planets (1991–2012)*, *106*(E10), 23,419–23,427.

Mitchell, D., C. Mazelle, J.-A. Sauvaud, J.-J. Thocaven, J. Rouzaud, A. Fedorov, P. Rouger, D. Toublanc, E. Taylor, D. Gordon, et al. (2016), The MAVEN solar wind electron analyzer, *Space Science Reviews*, *200*(1-4), 495–528.

Morgan, D. D., C. Dival, D. A. Gurnett, F. Duru, E. M. Dubinin, M. Fr?nz, D. J. Andrews, H. J. Opgenoorth, D. Ulu?en, I. Mitrofanov, and J. J. Plaut (2014), Effects of a strong ICME on the Martian ionosphere as detected by Mars Express and Mars Odyssey, *Journal of Geophysical Research: Space Physics*, *119*(7), 5891–5908, doi:10.1002/2013JA019522.

Morschhauser, A., V. Lesur, and M. Grott (2014), A spherical harmonic model of the lithospheric magnetic field of Mars, *Journal of Geophysical Research: Planets*, *119*(6), 1162–1188.

Opgenoorth, H. J., D. J. Andrews, M. Fr?nz, M. Lester, N. J. T. Edberg, D. Morgan, F. Duru, O. Witasse, and A. O. Williams (2013), Mars ionospheric response to solar wind variability, *Journal of Geophysical Research: Space Physics*, *118*(10), 6558–6587, doi:10.1002/jgra.50537.

Peterson, W., E. Thiemann, F. G. Eparvier, L. Andersson, C. Fowler, D. Larson, D. Mitchell, C. Mazelle, J. Fontenla, J. S. Evans, et al. (2016), Photoelectrons and solar ionizing radiation at Mars: Predictions versus MAVEN observations, *Journal of Geophysical Research: Space Physics*, *121*(9), 8859–8870.

Ramstad, R., S. Barabash, Y. Futaana, M. Yamauchi, H. Nilsson, and M. Holmstr?m (2017), Mars Under Primordial Solar Wind Conditions: Mars Express Observations of the Strongest CME Detected at Mars Under Solar Cycle #24 and its Impact on

Atmospheric Ion Escape, *Geophysical Research Letters*, *44*(21), 10,805–10,811, doi: 10.1002/2017GL075446, 2017GL075446.

Shane, A. D., S. Xu, M. W. Liemohn, and D. L. Mitchell (2016), Mars nightside electrons over strong crustal fields, *Journal of Geophysical Research: Space Physics*, *121*(4), 3808–3823.

Steckiewicz, M., C. Mazelle, P. Garnier, N. Andr, E. Penou, A. Beth, J.-A. Sauvaud, D. Toublanc, D. L. Mitchell, J. P. McFadden, J. G. Luhmann, R. J. Lillis, J. E. P. Connerney, J. R. Espley, L. Andersson, J. S. Halekas, D. E. Larson, and B. M. Jakosky (2015), Altitude dependence of nightside Martian suprathermal electron depletions as revealed by MAVEN observations, *Geophysical Research Letters*, pp. n/a–n/a, doi: 10.1002/2015GL065257, 2015GL065257.

Steckiewicz, M., P. Garnier, N. Andr, D. L. Mitchell, L. Andersson, E. Penou, A. Beth, A. Fedorov, J.-A. Sauvaud, C. Mazelle, D. A. Brain, J. R. Espley, J. McFadden, J. S. Halekas, D. E. Larson, R. J. Lillis, J. G. Luhmann, Y. Soobiah, and B. M. Jakosky (2017), Comparative study of the Martian suprathermal electron depletions based on Mars Global Surveyor, Mars Express, and Mars Atmosphere and Volatile EvolutioN mission observations, *Journal of Geophysical Research: Space Physics*, *122*(1), 857–873, doi:10.1002/2016JA023205, 2016JA023205.

Trotignon, J., C. Mazelle, C. Bertucci, and M. Acuna (2006), Martian shock and magnetic pile-up boundary positions and shapes determined from the Phobos 2 and Mars Global Surveyor data sets, *Planetary and Space Science*, *54*(4), 357–369.

Vennerstrom, S. (2011), Magnetic storms on mars, *Icarus*, *215*(1), 234 – 241, doi: https://doi.org/10.1016/j.icarus.2011.06.030.

Weber, T., D. Brain, D. Mitchell, S. Xu, J. Connerney, and J. Halekas (2017), Characterization of Low-Altitude Nightside Martian Magnetic Topology Using Electron Pitch Angle Distributions, *Journal of Geophysical Research: Space Physics*, *122*(10), 9777–9789, doi:10.1002/2017JA024491, 2017JA024491.

Xu, S., and M. W. Liemohn (2015), Superthermal electron transport model for Mars, *Earth and Space Science*, *2*(3), 47–64, doi:10.1002/2014EA000043, 2014EA000043.

Xu, S., M. W. Liemohn, and D. L. Mitchell (2014), Solar wind electron precipitation into the dayside Martian upper atmosphere through the cusps of strong crustal fields, *Journal of Geophysical Research: Space Physics*, *119*(12), 10,100–10,115, doi: 10.1002/2014JA020363.

Xu, S., M. W. Liemohn, W. Peterson, J. Fontenla, and P. Chamberlin (2015a), Comparison of different solar irradiance models for the superthermal electron transport model for Mars, *Planetary and Space Science*, *119*, 62–68.

Xu, S., M. Liemohn, S. Bougher, and D. Mitchell (2015b), Enhanced carbon dioxide causing the dust storm-related increase in high-altitude photoelectron fluxes at Mars, *Geophysical Research Letters*, *42*(22), 9702–9710.

Xu, S., D. Mitchell, M. Liemohn, C. Dong, S. Bougher, M. Fillingim, R. Lillis, J. McFadden, C. Mazelle, J. Connerney, and B. Jakosky (2016a), Deep nightside photoelectron observations by MAVEN SWEA: Implications for Martian northern hemispheric magnetic topology and nightside ionosphere source, *Geophysical Research Letters*, *43*(17),

8876–8884, doi:10.1002/2016GL070527, 2016GL070527.

Xu, S., M. Liemohn, S. Bougher, and D. Mitchell (2016b), Martian high-altitude photoelectrons independent of solar zenith angle, *Journal of Geophysical Research: Space Physics*, *121*(4), 3767–3780, doi:10.1002/2015JA022149, 2015JA022149.

Xu, S., D. Mitchell, M. Liemohn, X. Fang, Y. Ma, J. Luhmann, D. Brain, M. Steckiewicz, C. Mazelle, J. Connerney, and B. Jakosky (2017a), Martian low-altitude magnetic topology deduced from MAVEN/SWEA observations, *Journal of Geophysical Research: Space Physics*, pp. n/a–n/a, doi:10.1002/2016JA023467, 2016JA023467.

Xu, S., D. Mitchell, J. Luhmann, Y. Ma, X. Fang, Y. Harada, T. Hara, D. Brain, T. Webber, C. Mazelle, and G. A. DiBraccio (2017b), High-altitude closed magnetic loops at Mars observed by MAVEN, *Geophysical Research Letters*, pp. n/a–n/a, doi:10.1002/2017GL075831, 2017GL075831.

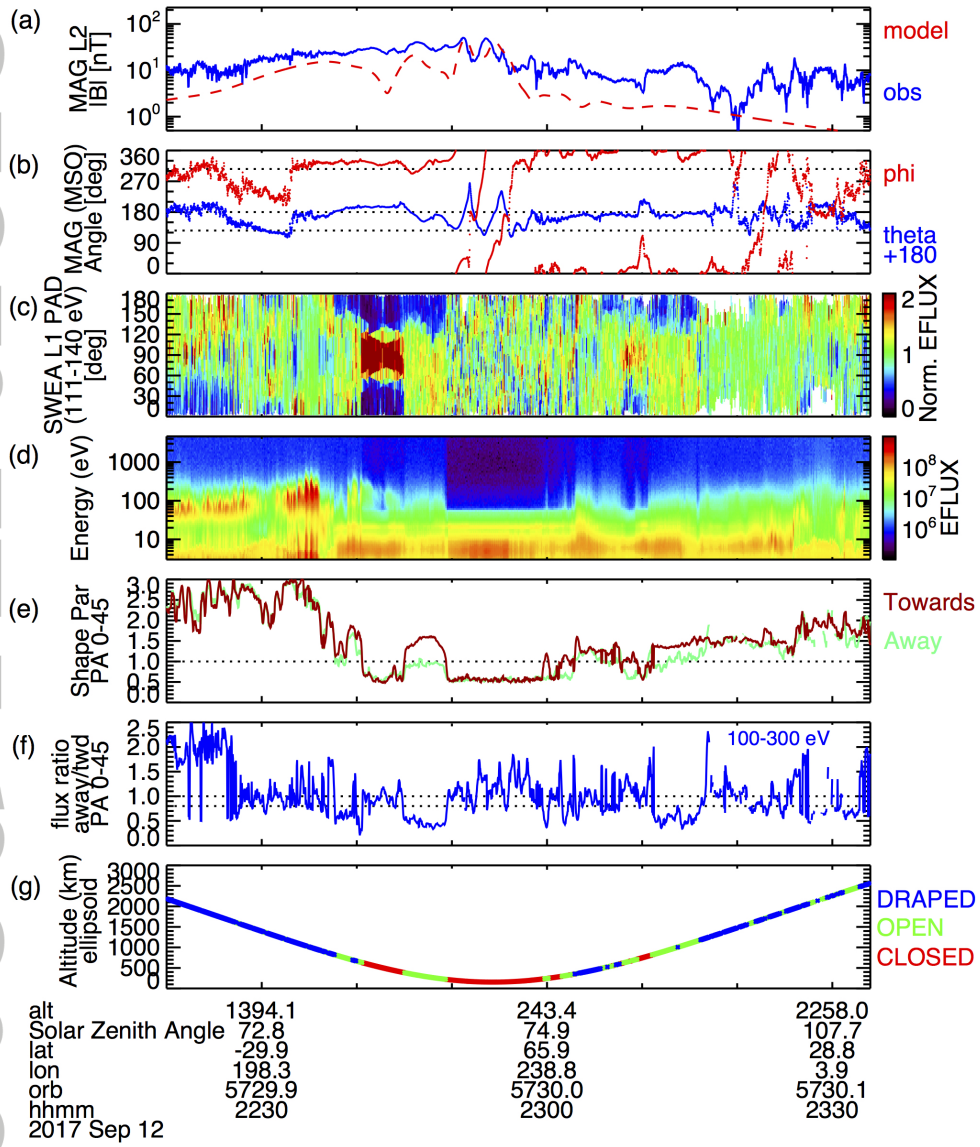

Figure 1. Time series on Sep. 12, 2017 of (a) magnetic field magnitude (blue) and (b) angles in the Mars-centered Solar Orbital (MSO) coordinates measured by MAG, (c) pitch angle distribution (PAD) of 111-140 eV electrons normalized by the median electron flux and (d) electron energy spectra (in differential energy flux: $eVsr^{-1}cm^{-2}s^{-1}eV^{-1}$) measured by SWEA, (e) pitch angle-resolved shape parameters, (f) flux ratio of "away" and "toward" electrons for 100-300 eV, and (g) spacecraft altitude colored by magnetic topologies. The MSO coordinates are defined as: X points from the center of Mars to the Sun; Y is opposite to the orbital motion of Mars; Z completes the right-hand rule, perpendicular to the Mars' orbital plane. In (a), the modeled magnetic field magnitude in dashed red is from *Morschhauser et al.* [2014]. In (b), the phi angle is the azimuthal angle in MSO, pointing from X-axis to Y-axis, and the theta angle is the elevation angle relative to the X-Y plane but shifted by 180°.

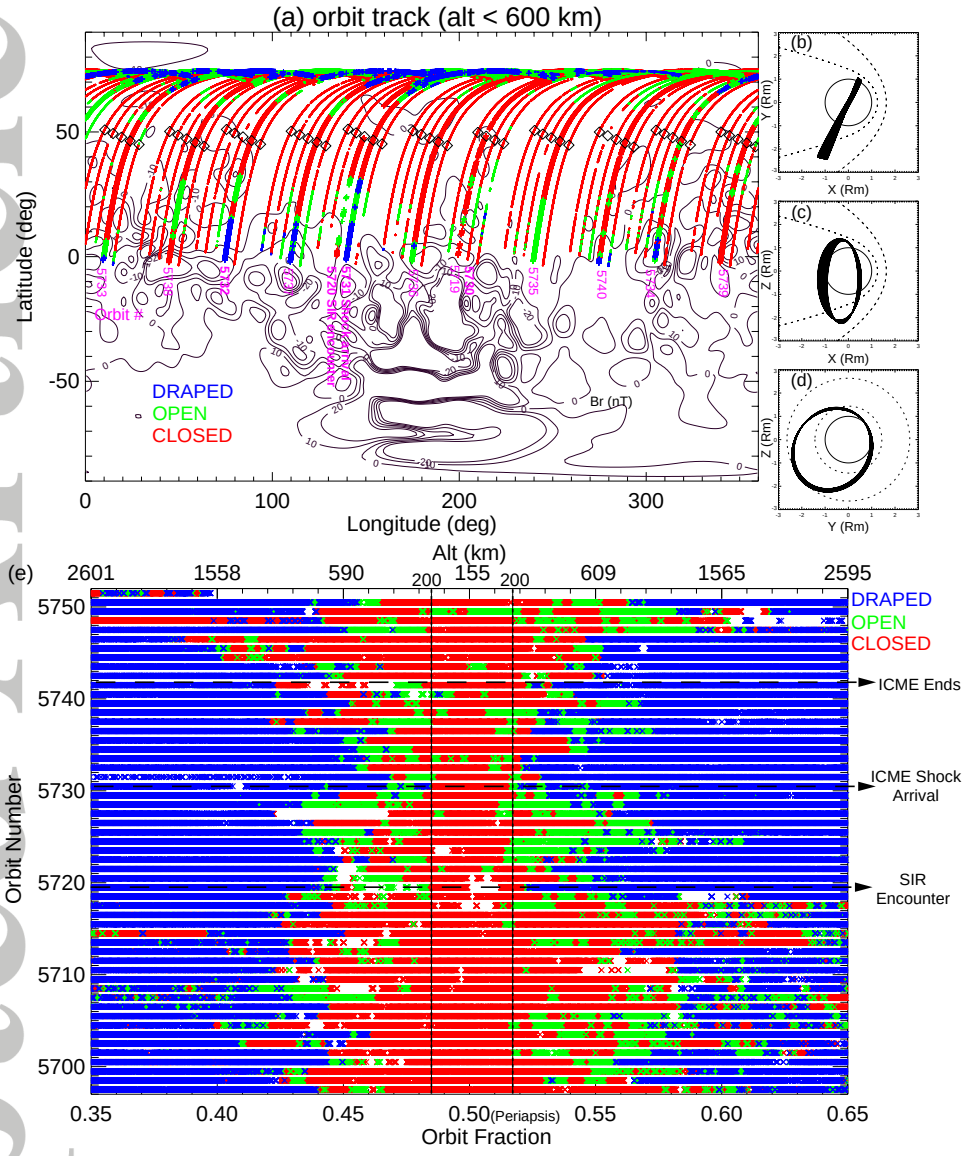

Figure 2. (a) MAVEN orbit tracks, colored by magnetic topologies, from Sep. 7 to Sep. 17, 2017 (orbits 5698-5751), only altitude below 600 km shown. Orbit numbers are shown in magenta. Dimond symbols mark the periapsis location of each orbit. The contours are radial magnetic fields at 400 km based on the crustal field model from *Morschhauser et al.* [2014]. Orbit geometry in MSO (b) X-Y, (c) X-Z, and (d) Y-Z plane for the same time period. The dotted lines are empirical bow shock (outer lines) and magnetic pileup boundary (inner lines) locations based on parameters from *Trotignon et al.* [2006]. (e) Magnetic topology from Sep. 7 to Sep. 17, 2017, with the X axis being the orbit fraction (0-0.5 for inbound and 0.5-1 for outbound) and the Y axis being the orbit number shift by 0.5. For example, periapsis of 5731 is decomposed into X=0.5 and Y=5730.5. Blanks in magnetic topology are caused by insufficient PA coverages. The two vertical dashed lines mark 200 km in altitude.

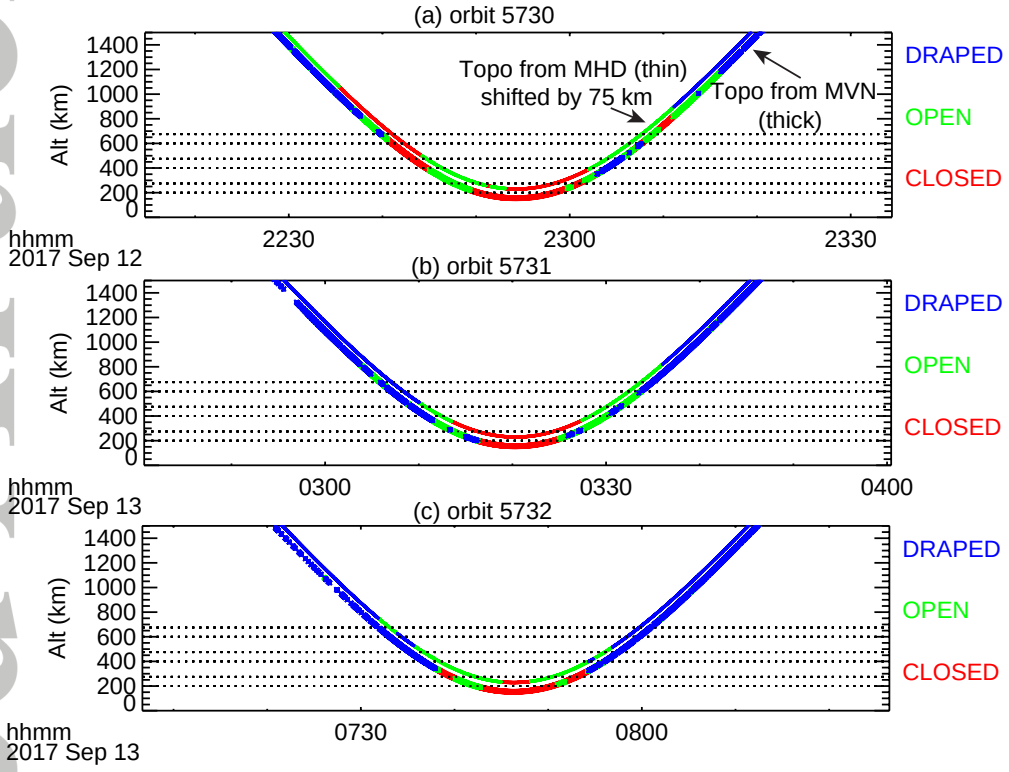

Figure 3. The comparison of magnetic topology determined from MAVEN data (thick lines) and from MHD simulations (thin lines). Magnetic topology from MHD is shifted 75 km upward in altitude. The three panels correspond to the orbit segment near periapsis before the shock arrival (a, orbit 5370), right after the shock arrival (b, orbit 5371), and one orbit after (c, orbit 5372). These dashed lines mark altitudes of 200, 275, 400, 475, 600, and 675 km.

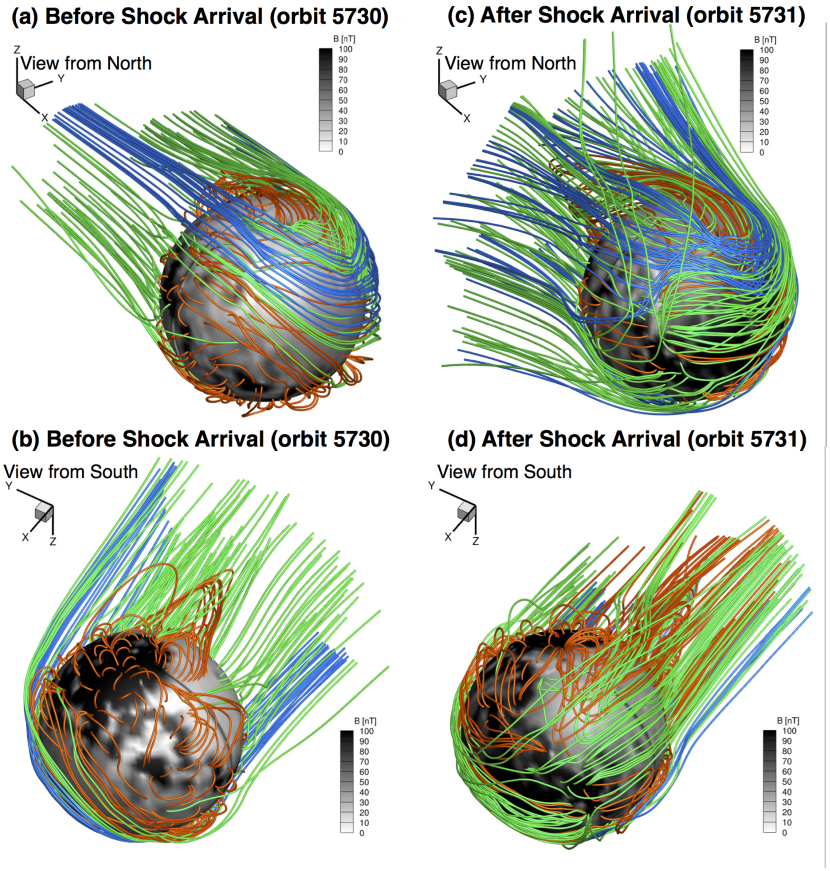

Figure 4. The comparison of global magnetic topology from the time-dependent MHD simulation before the shock arrival (orbit 5370) at 2017-09-12/22:40 (a and b) and after the shock arrival (orbit 5371) at 2017-09-13/03:05 (c and d). The top two panels (a and c) are viewed from the north and the bottom two (b and d) from the south. The field lines are traced over a spherical surface at 350 km altitude with a 15°×15° longitude-latitude grid. The blue/green/orange colors indicate draped/open/closed field lines, respectively. The gray color indicates the magnetic field strength at 110 km altitude (including both crustal and induced field components).